

Article

Integrating Real-Time Meteorological Conditions into a Novel Fire Spread Model for Grasslands

Yakun Zhang ¹, Huimin Yu ¹, Wenjiang Huang ^{2,3} , Tiecheng Huang ^{2,3} , Meng Fan ²  and Kun Wang ^{2,*} 

¹ School of Mathematics and Statistics, Shandong Normal University, Jinan 250014, China; 2022020496@stu.sdnu.edu.cn (Y.Z.); hmyu@sdnu.edu.cn (H.Y.)

² State Key Laboratory of Remote Sensing Science, Aerospace Information Research Institute, Chinese Academy of Sciences, Beijing 100094, China; huangwj@aircas.ac.cn (W.H.); huangtc@aircas.ac.cn (T.H.); fanmeng@aircas.ac.cn (M.F.)

³ University of Chinese Academy of Sciences, Beijing 100049, China

* Correspondence: wangk@aircas.ac.cn

Abstract: Accurate comprehension of grassland fires is imperative for maintaining ecological stability. In this study, we propose a novel fire model that incorporates real-time meteorological conditions. Our methodology integrates key meteorological factors including relative humidity, temperature, degree of solidification of combustible materials, and wind speed. These factors are embedded into a comprehensive function that determines both the downwind and upwind spreading speeds of the fire. Additionally, the model accommodates fire spread in the absence of wind by incorporating the direction perpendicular to the wind, with wind speed set to zero. By precisely determining wind speed, the model enables real-time calculation of fire spread speeds in all directions. Under stable wind conditions, the fire spread area typically adopts an elliptical shape. Leveraging ellipse properties, we define the aspect ratio as a function related to wind speed. Consequently, with knowledge of the fire duration, the model accurately estimates the area of fire spread. Our findings demonstrate the effectiveness of this model in predicting and evaluating fires in the Hulunbuir Grassland. The model offers an innovative method for quantifying grassland fires, contributing significantly to the understanding and management of grassland ecosystems.

Keywords: fire behavior; interconnected model; fire spread speed; environmental factor



Citation: Zhang, Y.; Yu, H.; Huang, W.; Huang, T.; Fan, M.; Wang, K. Integrating Real-Time Meteorological Conditions into a Novel Fire Spread Model for Grasslands. *Fire* **2024**, *7*, 154. <https://doi.org/10.3390/fire7050154>

Academic Editors: Yanming Ding, Kazui Fukumoto and Jiaqing Zhang

Received: 2 April 2024
Revised: 24 April 2024
Accepted: 25 April 2024
Published: 26 April 2024



Copyright: © 2024 by the authors. Licensee MDPI, Basel, Switzerland. This article is an open access article distributed under the terms and conditions of the Creative Commons Attribution (CC BY) license (<https://creativecommons.org/licenses/by/4.0/>).

1. Introduction

Grasslands cover approximately 40% of the Earth's total land area [1]. In China, grasslands account for 41.4% of the country's land area [2]. They are rich in water, carbon, and energy resources, making them significant contributors to carbon balance, environmental protection, and industrial production [3,4]. As an integral component of ecosystem succession, wildfires have the potential to significantly impact terrestrial and global ecosystems [5]. These events can lead to alterations in the composition and structure of vegetation within ecosystems, as well as influence climate change and the carbon cycle. Grassland fire is a crucial ecological factor in grassland ecosystems and has a profound impact on their development, succession, and extinction [6,7]. While the proper use of fire resources can yield positive ecological outcomes, uncontrolled fires pose a significant threat to public safety and property [6,8].

Grassland fires are destructive, widespread, and challenging to extinguish and mitigate [9]. Their frequent occurrence has adverse effects on the grassland ecosystem, such as increased soil water evaporation, hindrance of vegetation regrowth, and loss of vegetation cover [10]. To gain a comprehensive understanding of the spatial and temporal distribution of grassland fires and their spread and impact, it is essential to manage fires in a scientific, effective, and rational manner [11,12]. This underscores the importance of studying fires scientifically. Global warming is believed to exacerbate the severity and frequency of

wildfires in both the short and long term, thereby increasing their hazardousness [13–15]. Simultaneously, climate plays a crucial role in influencing the flammability and availability of fuels [16,17]. Given the significant impact of climate on fire dynamics [18,19], it becomes imperative to quantify the influence of climatic factors on wildfires, to enhance prevention and ensure an effective response to fire incidents [20,21].

Grassland fires have a significant impact on global vegetation change and carbon balance, making them a crucial focus of current research [7]. Various parameters are used to quantify the magnitude of the fire, including fire spread rate, fire area, and fire radiation intensity [22]. Numerous studies have been conducted to describe, measure, and model these parameters [22]. The first empirically based model of fire behavior was proposed by McArthur and is still widely used today with some adjustments and refinements [23]. Cheney further developed this model and established a parameterization model for fire, which includes equations describing the relationship between wind speed and fire spread rate, as well as other environmental factors such as temperature and relative humidity [24]. Zhou updated the model parameters by applying Cheney's model to a mowing field [25]. Miguel improved the model parameters based on Cheney's model and used linear regression to establish the relationship between critical wind speed and fire spread rate, demonstrating that the magnitude of wind speed influences fire spread rate [26]. Although this model provides a simple way to determine fire spread rate based on wind speed, it does not consider fire area.

In contrast, Arroa et al. differentiated fire spread rate based on wind direction, dividing it into downwind spread rate, upwind spread rate, and spread rate perpendicular to the wind direction [27]. Assuming the fire area to be an ellipse, they used the aspect ratio of the ellipse to establish a link between downwind spread rate and spread rate perpendicular to the wind direction. This allowed them to construct a relationship between fire area and downwind spread rate. Li further improved this model by incorporating the head-to-head ratio of the ellipse as a parameter, successfully establishing the relationship between downwind spread rate and upwind spread rate, thus refining the model [28]. However, this model is more suitable for large-scale applications, and the accuracy of fire spread rate calculations may be insufficient. Additionally, the influence of temperature on fire is not considered in this model.

In this paper, Li's and Miguel's models are coupled to establish a model of fire response to the environment on a small scale, and the Hulunbuir Grassland fire is used as an example for validation. The model covers variables such as temperature, relative humidity, critical wind speed, etc. Under the assumption that the fire area is an ellipse, the nature of the ellipse is utilized to establish the relationship between the environmental factors and the fire spreading speed, the relationship within the fire spreading speed, and finally, the relationship between the environmental factors and the area is obtained, and several specific functions are formed. The paper's structure is summarized as follows. Section 2 introduces a pioneering parametric coupled model for fire, while Section 3 elaborates on the results utilized to compare our model with existing ones and scrutinizes the outcomes. The conclusion is then presented in the final section.

2. Materials and Methods

In this section, we introduce a model tailored for small-scale scenarios, enabling precise quantification of individual fires. The model delivers real-time estimations of fire spread rate and area, contributing to an improved understanding of fire behavior and the facilitation of effective fire control measures. The subsequent discussion will initially outline the process of parameterizing the model, elucidating the construction of the framework by integrating the existing model and coupling it to create a novel model. Subsequently, the input, process, and output variables of the model will be precisely specified.

2.1. The Fuel Moisture ϕ_M

The parameterization process of the model involves quantifying the effects of temperature and relative humidity on the occurrence and spread of fire. Both these factors play a significant role in determining the likelihood and rate of fire propagation.

To quantify the effect of temperature, the model considers the evaporation of water from combustible materials. As the temperature increases, the evaporation rate also increases, leading to a higher possibility of fire. However, it is important to note that a certain starting temperature is required for the occurrence of fire.

Relative humidity also plays a crucial role in fire occurrence and spread. When the humidity exceeds 70%, it becomes difficult for fires to occur. Higher levels of humidity inhibit the evaporation of water from combustible materials, reducing the likelihood of ignition.

In order to incorporate the effects of temperature and relative humidity into the model, the fine dead grass moisture content (MC) is used. This parameter represents the amount of moisture present in the fine dead grass, which is a key factor in determining the flammability of the grass. By quantifying the moisture content, the model can accurately assess the likelihood and rate of fire spread.

The fine dead grass moisture content MC (%) [24] is:

$$MC = 9.58 - 0.205T + 0.138RH \tag{1}$$

where T is the temperature ($^{\circ}C$), RH is the relative humidity (%).

The fuel moisture ϕ_M (Figure 1) [24] is estimated by

$$\phi_M = \begin{cases} e^{-0.108MC}, & MC < 12\% \\ 0.684 - 0.0342MC, & MC \geq 12\%, w < 10 \text{ km} \cdot \text{h}^{-1} \\ 0.547 - 0.0228MC, & MC \geq 12\%, w \geq 10 \text{ km} \cdot \text{h}^{-1} \end{cases} \tag{2}$$

The specific functional equation is

$$\phi_M = \begin{cases} e^{0.02214T - 0.014904RH - 1.03464}, & MC < 12\% \\ 0.007011T - 0.0047196RH + 0.356364, & MC \geq 12\%, w < 10 \text{ km} \cdot \text{h}^{-1} \\ 0.004674T - 0.0031464RH + 0.328576, & MC \geq 12\%, w \geq 10 \text{ km} \cdot \text{h}^{-1} \end{cases} \tag{3}$$

where w is the instantaneous near-surface (10 m) wind speed ($\text{km} \cdot \text{h}^{-1}$). ϕ_M can reflect the influence of the real-time weather conditions on fire. As can be seen from the formula, its impact on fire is also restricted by wind speed.

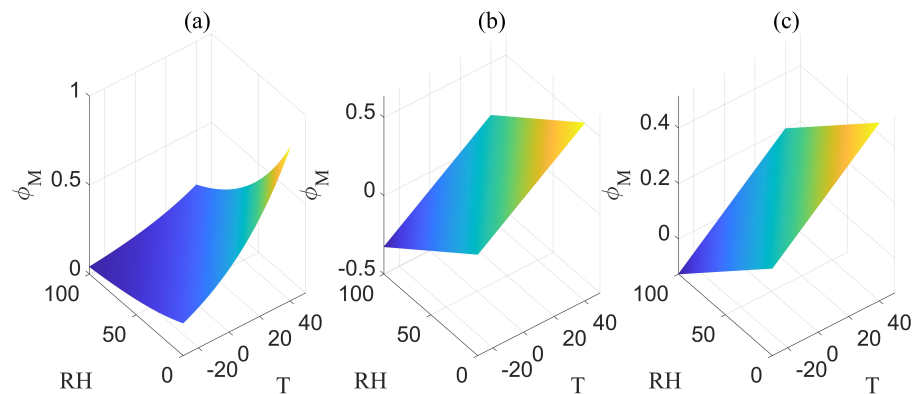


Figure 1. (a) The image of ϕ_M is obtained when the moisture content (MC) is less than 12%. (b) The image of ϕ_M is obtained when the moisture content (MC) is greater than or equal to 12% and the wind speed (w) is less than $10 \text{ km} \cdot \text{h}^{-1}$. (c) The image of ϕ_M is obtained when the moisture content (MC) is greater than or equal to 12% and the wind speed (w) is greater than or equal to $10 \text{ km} \cdot \text{h}^{-1}$.

2.2. The Effect of the Curing Coefficient ϕ_C

The following formula is to quantify the effect of the curing coefficient [24].

$$\phi_C = \frac{1.036}{1 + 103.99e^{-0.0996(c-20)}} \tag{4}$$

where c is the degree of curing of grass (%).

In Hulunbuir Grassland, fires are more likely to occur between May and October. The condition of the grass plays a significant role in fire occurrence, with fires typically not occurring when the grass is less than 20% cured. In fact, the degree of grass curing directly influences the probability of fire occurrence. As the degree of grass curing increases, the likelihood of fire occurrence also increases.

2.3. the Effect of Wind Speed on Fire Speed

Upon establishing the influence of meteorological and fuel conditions on fire behavior, the subsequent analysis focuses on the impact of wind speed on fire spread.

The fire burning area is conceptualized as an ellipse, with the wind direction representing the major axis and the direction perpendicular to the wind direction representing the minor axis. The ignition point of the fire is positioned at the focal point of the major axis. This configuration is visually depicted in Figure 2.

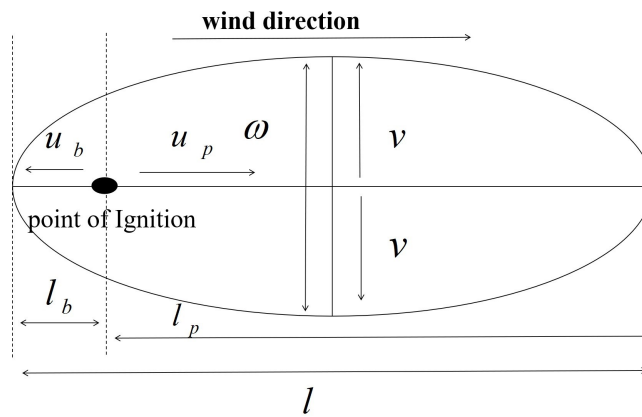


Figure 2. The shape of the fire burning area.

Given a specific wind direction, the speed at which the fire spreads is illustrated in the following diagram.

$$l = l_p + l_b \tag{5}$$

$$\frac{dl_p}{dt} = u_p, \quad \frac{dl_b}{dt} = u_b, \quad \frac{d\omega}{dt} = 2v \tag{6}$$

where l is the length of the major axis, ω is the length of the short axis. u_p is the downwind speed, and u_b is the upwind speed. The downwind spread speed of the fire is directly influenced by the wind speed, with higher wind speeds resulting in a greater downwind spread speed. On the other hand, the upwind spread speed is a fraction of the wind speed. Additionally, the natural spread speed of the fire, denoted as v , remains independent of the wind speed.

By adopting the focal point as the origin and employing the long and short axes as the coordinate system, the spreading velocity of individual points at the periphery of the burning area can be ascertained (Figure 3). As an illustrative example, we shall consider point E .

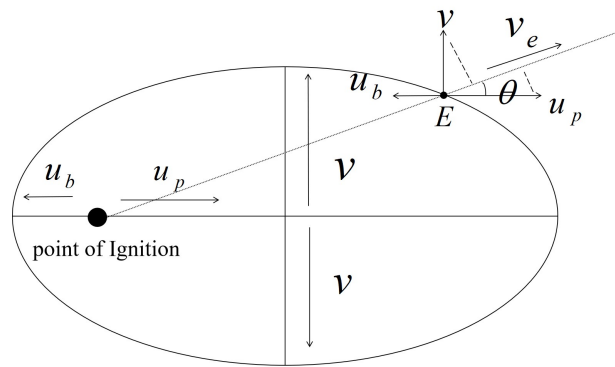


Figure 3. Spreading velocity analysis of the burning area periphery.

Hence,

$$v_e = u_p \cos \theta + v \sin \theta - u_b \cos \theta$$

Here, θ represents the angle formed by the line connecting the point and the fire point with the long axis.

Notably, when $w = 0$, all points exhibit identical velocities. Consequently, the burning area assumes a circular shape with the fire point serving as its center. In this scenario, the equations undergo the following modifications:

$$L_B = 1, u_p = u_b = v, v_e = v \cos \theta$$

$$a = v^2 \pi \tau^2$$

Assuming the fire spread area takes the shape of an ellipse, the ratio of its length to breadth (L_B) determines the shape of the ellipse. In this study, the L_B ratio is associated with the fire speed, thus influencing the overall shape of the fire spread area.

$$L_B = \frac{l}{\omega} = \frac{l_p + l_b}{\omega} = \frac{u_p + u_b}{2v} \tag{7}$$

In this study, we let

$$L_B = 1.063w^{0.473} \tag{8}$$

where w is the instantaneous near-surface (10 m) wind speed.

2.4. The Fire Spread Speed

In the subsequent analysis, the rate of fire spread is classified into three categories based on the correlation between the rate of fire spread and the direction of the wind: downwind spread, upwind spread, and perpendicular to the wind of spread. The specific details are elaborated upon below.

2.4.1. The Downwind Spread u_p

The downwind spread rate is most affected by the wind speed at the time of the fire [26]. It is given as

$$u_p = \begin{cases} (0.054 + 0.209w)\phi_M\phi_C, & w < 5 \text{ km} \cdot \text{h}^{-1} \\ (1.1 + 0.705(w - 5)^{0.844})\phi_M\phi_C, & w \geq 5 \text{ km} \cdot \text{h}^{-1} \end{cases} \tag{9}$$

By utilizing this model, a more comprehensive depiction of the influence of wind speed on fire behavior can be elucidated.

Where

$$\phi_M = \begin{cases} e^{-0.108MC}, & MC < 12\% \\ 0.684 - 0.0342MC, & MC \geq 12\%, w < 10 \text{ km} \cdot \text{h}^{-1} \\ 0.547 - 0.0228MC, & MC \geq 12\%, w \geq 10 \text{ km} \cdot \text{h}^{-1} \end{cases} \quad (10)$$

$$\phi_C = \frac{1.036}{1 + 103.99e^{-0.0996(c-20)}} \quad (11)$$

2.4.2. The Fire Spread Speed Perpendicular to the Wind Direction v

In this modeling, we assume that under conditions of complete stillness, where there is no wind ($w = 0$), the fire will originate at the fire point and spread uniformly to the surrounding area at a consistent rate. After a certain period of time, the overfire area will take on a circular shape. The rate of spread perpendicular to the wind direction remains similar to that in the absence of wind, as both rates are unaffected by wind. Thus, we consider the rate of fire spread in the absence of wind to be equivalent to the rate of fire spread perpendicular to the wind direction. Thus, The fire spread speed perpendicular to the wind direction v is

$$v = u_p, \text{ when } w = 0 \\ = \begin{cases} 0.054\phi_M\phi_C, & w < 5 \text{ km} \cdot \text{h}^{-1} \\ (1.1 + 0.705(-5)^{0.844})\phi_M\phi_C, & w \geq 5 \text{ km} \cdot \text{h}^{-1} \end{cases} \quad (12)$$

The functional equation that governs the proposed model can be expressed as follows:

$$v = \begin{cases} \frac{0.055944e^{0.02214T-0.014904RH-1.03464}}{103.99e^{1.992-0.0996c} + 1}, & MC < 12\% \\ \frac{0.055944(0.007011T - 0.0047196RH + 0.356364)}{103.99e^{1.992-0.0996c} + 1}, & MC \geq 12\%, w < 10 \text{ km} \cdot \text{h}^{-1} \\ \frac{0.055944(0.004674T - 0.0031464RH + 0.328576)}{103.99e^{1.992-0.0996c} + 1}, & MC \geq 12\%, w \geq 10 \text{ km} \cdot \text{h}^{-1} \end{cases} \quad (13)$$

2.4.3. The Upwind Spread u_b

Combined with Equations (3)–(12), u_b can be expressed in the following form.

$$u_b = 2L_B v - u_p \quad (14)$$

We define

$$\lambda(T, RH) = \begin{cases} e^{0.02214T-0.014904RH-1.03464}, & MC < 12\% \\ (0.007011T - 0.0047196RH + 0.356364), & MC \geq 12\%, w < 10 \text{ km} \cdot \text{h}^{-1} \\ (0.004674T - 0.0031464RH + 0.328576), & MC \geq 12\%, w \geq 10 \text{ km} \cdot \text{h}^{-1} \end{cases} \quad (15)$$

$$\gamma(c) = \frac{1}{(103.99e^{1.992-0.0996c} + 1)} \quad (16)$$

$$\delta(w) = \begin{cases} 0.118937w^{0.473} - 1.036(0.209w + 0.054), & w < 5 \text{ km} \cdot \text{h}^{-1} \\ 0.118937w^{0.473} - 1.036(0.705(w - 5)^{0.844} + 1.1), & w \geq 5 \text{ km} \cdot \text{h}^{-1} \end{cases} \quad (17)$$

Through the process of calculation, we derive a precise formula for the parameter u_b as follows:

$$u_b = \lambda(T, RH)\gamma(c)\delta(w) \quad (18)$$

2.5. The Area of Fire Spread *s*

In summary, by integrating the functions of u_p , u_b , and v with temperature, wind speed, relative humidity, and the degree of grass curing, along with the duration of the fire occurrence, it becomes possible to obtain a comprehensive understanding of the area of fire spread and its relationship to these variables.

With fire duration of time τ , the fire burning area can be described as

$$s = \pi \frac{l}{2} \frac{\omega}{2} = \frac{\pi}{2} (u_p + u_b) v \tau^2 \tag{19}$$

The function can be found that all these factors (temperature, relative humidity, wind speed, and the degree of curing of grass) have a direct effect on the fire spread area. We can extract the formula for the effect of each factor on the fire spread area. Among them, the influence of relative humidity and temperature on the fire spread area is the most complex.

We define

$$\lambda^2(T, RH) = \begin{cases} e^{0.04428T - 0.029808RH - 2.06928}, & MC < 12\% \\ (0.007011T - 0.0047196RH + 0.356364)^2, & MC \geq 12\%, w < 10 \text{ km} \cdot \text{h}^{-1} \\ (0.004674T - 0.0031464RH + 0.328576)^2, & MC \geq 12\%, w \geq 10 \text{ km} \cdot \text{h}^{-1} \end{cases} \tag{20}$$

$$\mu(c) = \frac{0.0033269}{(103.99e^{1.992 - 0.0996c} + 1)^2} \tag{21}$$

$$\kappa(w) = w^{0.473} \tag{22}$$

Therefore, the function of the area of fire spread can be formulated in terms of this variable.

$$s = \lambda^2(T, RH) \mu(c) \kappa(w) \pi \tau^2 \tag{23}$$

The image of the influence function of each factor can be seen in the figure below. The correlation between fire area and this influencing factor can be clearly seen based on their images (Figures 4 and 5).

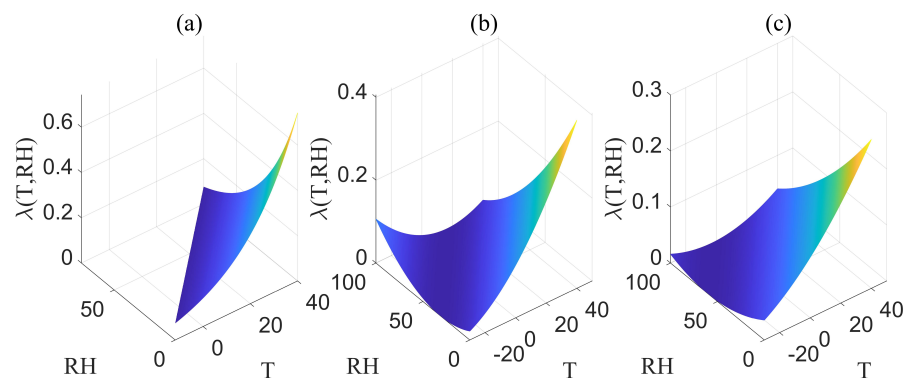


Figure 4. (a) The image of λ is obtained when the moisture content (MC) is less than 12%. (b) The image of λ is obtained when the moisture content (MC) is greater than or equal to 12% and the wind speed (w) is less than $10 \text{ km} \cdot \text{h}^{-1}$. (c) The image of λ is obtained when the moisture content (MC) is greater than or equal to 12% and the wind speed (w) is greater than or equal to $10 \text{ km} \cdot \text{h}^{-1}$.

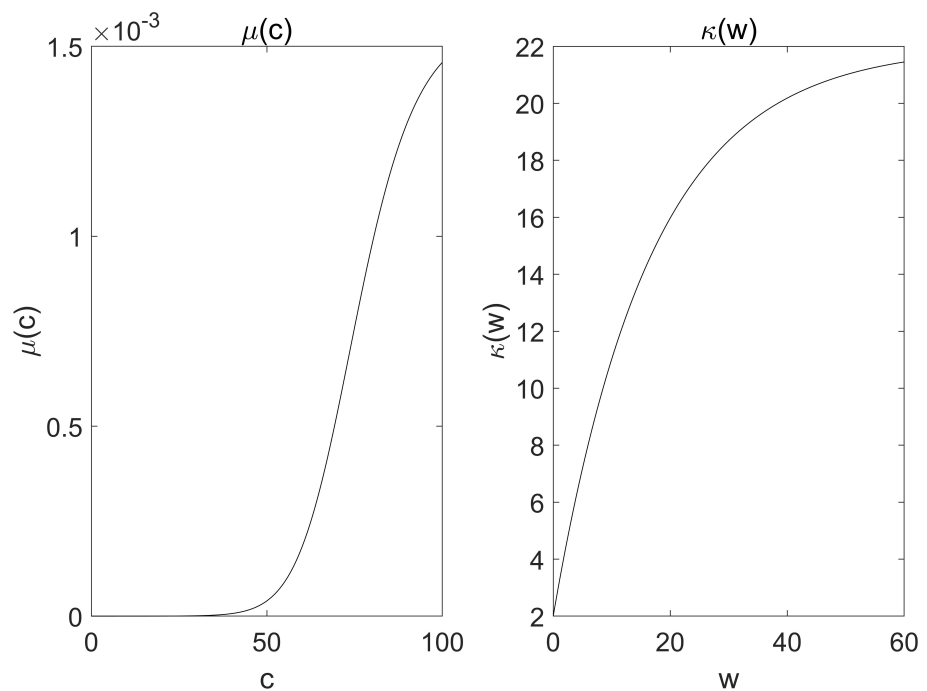


Figure 5. The visualization of $\mu(c)$ and $\kappa(w)$.

2.6. Modeling Process

The fire parameterization scheme proposed in this study (Figure 6) involves four input variables: wind speed (w), relative humidity (RH), temperature (T), and grass curing degree (c). Assuming the fire area can be approximated as an ellipse, the length-to-breadth ratio (L_B) of the fire spread area can be determined based on the wind speed. The relative humidity and temperature values are used to estimate the fine dead grass moisture content (MC) and fuel moisture (ϕ_M), respectively. Additionally, the curing coefficient (ϕ_C) is derived from the grass curing degree. Using these calculated parameters, different functions are employed to determine the corresponding fire spread speeds. The fire spread area is then obtained by considering the average fire spread speed and the duration of the fire occurrence.

All factors, including temperature, relative humidity, wind speed, and the degree of grass curing, have a direct impact on the fire spread area. Through data analysis and further research, it is possible to derive formulas that quantify the effect of each factor on the fire spread area.

However, it is important to note that the influence of relative humidity and temperature on the fire spread area tends to be more complex and multifaceted compared to other factors. Relative humidity affects the moisture content of the fuel, which in turn affects its flammability. Higher relative humidity can inhibit the spread of fire by reducing the fuel's ability to ignite and sustain combustion. Conversely, lower relative humidity can increase the fire spread area due to drier fuel conditions.

Similarly, temperature plays a critical role in fire behavior. Higher temperatures can accelerate fuel drying, making it more susceptible to ignition and promoting faster fire spread. Additionally, higher temperatures can enhance convective heat transfer, leading to more intense fire behavior and larger fire spread areas.

The wind exerts a definitive influence on the speed and spatial extent of fire propagation in all directions, significantly impacting the shape and dimensions of the fire spread area. Higher wind speeds correspond to increased downwind spread rates and expanded downwind spread areas, resulting in the elongation of the major axis of the fire spread area, as demonstrated by a more "flattened" ellipse in graphical representations.

To derive precise formulas for the effect of relative humidity, temperature, wind speed, etc. on the fire spread area, extensive research, data analysis, and modeling techniques are typically employed. These formulas take into account the complex interactions between these factors, as well as other variables, to provide a comprehensive understanding of their influence on fire spread.

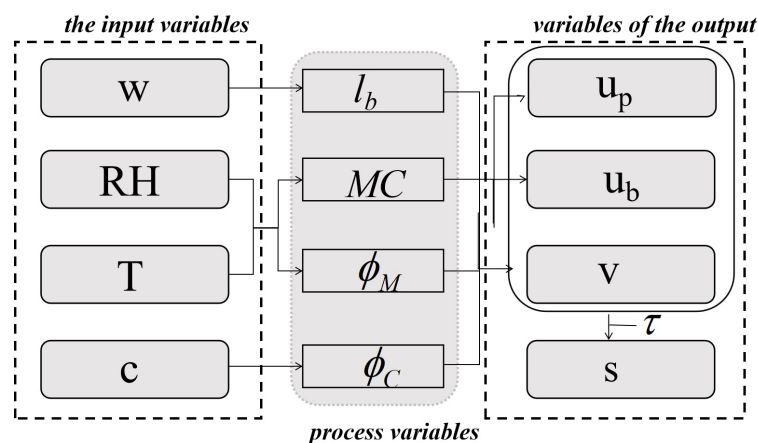


Figure 6. Input, process, and output variables in the model.

3. Results and Discussion

3.1. Test Sites

The Hulunbuir Grassland (47.08°–53.23° N, 115.22°–126.06° E) is situated in the north-eastern part of the Inner Mongolia Autonomous Region, and forms a part of the Mongolian Plateau. The topography is characterized by slightly higher terrain in the southeast, sloping gently towards the northwest, and slightly lower elevation in the central region [29]. The climate is classified as temperate continental monsoon, with an average annual temperature ranging from -3 to 0 °C and annual precipitation of 250 to 400 mm [30]. Abundant water resources are present in the region, encompassing over 3000 large and small rivers as well as more than 500 lakes. The total grassland area spans 6.71 million hectares, constituting 12.36% of the entire grassland area within the autonomous region. The vegetation cover of the grasslands in Hulunbuir City, where the grassland is situated, is recorded at 76.15% (2023). The vegetation types within the area range from temperate meadow grassland and temperate typical grassland in the east to low flatland meadows, mountain meadows, and swamps in the west. Hulunbuir Grassland is a renowned tourist destination and a crucial hub for scientific research vulnerable to fire disasters.

On average, the region experiences around 430 grass fires per year, resulting in a total overfire area of about 1,111,717 hectares [31]. Human-caused fires are the dominant type in this area, with the highest frequency occurring in March and April, making spring and summer the most fire-prone seasons. Fires pose a significant threat in Hulunbuir, leading to substantial economic losses, endangering human life and health, and resulting in a considerable waste of financial and material resources as well as manpower.

In Inner Mongolia, the heightened wildfire activity occurs predominantly from March through April, coinciding with the transition from winter to spring in the Northern Hemisphere, marked by a gradual warming trend. Notably, northeastern China experiences a corresponding escalation in wildfire occurrences during this period [32]. Simultaneously, the absence of East Asian summer winds over China results in predominantly sunny and dry weather conditions, driven by high-pressure systems, which are conducive to wildfire incidents. Inner Mongolia's arid climate, characterized by minimal spring rainfall and rising temperatures, accelerates water vapor evaporation and fosters vigorous vegetation growth. These conducive growth conditions facilitate the accumulation of combustible materials from the flourishing vegetation [33], significantly heightening the probability of wildfires.

3.2. The Dataset

We conducted a selection of 29 fires that occurred in the Hulunbuir Grassland between 2012 and 2016 to validate the proposed model. These fires were observed to transpire predominantly from March to October, with a notable concentration in the months of March and April. The assessment of fire size necessitates a quantifiable indicator, and in this context, fire radiative power (FRP) emerges as a pivotal parameter for gauging fire intensity. Fire radiative power has been widely used as a proxy for fire intensity. It can be used to characterize fire types, fire behavior, and fire states to predict fire danger [34]. This variable is retrieved from the radiance at the 4 μm band of satellite sensors and represents the instantaneous radiative energy that is released from actively burning fires. The latest MODIS Collection 6 active fire product provides more scientifically reliable fire detections and FRP retrievals [35]. Notably, higher FRP values correspond to heightened fire intensity and a subsequent increase in associated damage. The fire radiative power of the selected fires exhibited a range from 0.52 to 85.3 (MW), with an average value of 15.5 (MW). Detailed information about the four parameters (w , RH , c , T) utilized in this model for the selected data is expounded upon in the subsequent section. The fire parameterized model was validated using data from 29 fires that occurred in the Hulunbuir Grassland, as shown in Figure 7.

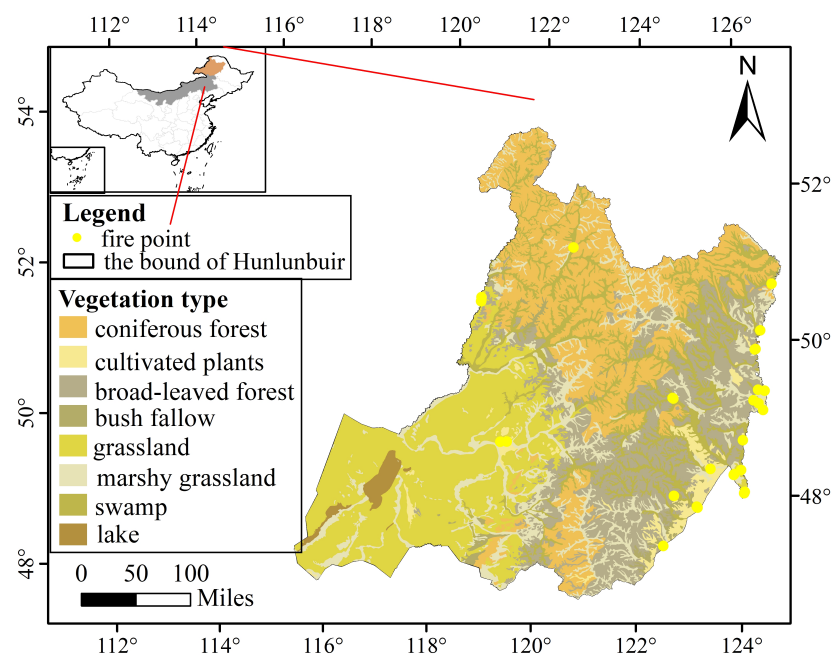


Figure 7. The fires occurring in the Hulunbuir Grassland.

The data used in the study included instantaneous near-surface air temperature (T , in degrees Celsius) and instantaneous near-surface wind speed (w , in kilometers per hour) obtained from the China Meteorological Forcing Dataset (CMFD) [36,37]. The spatial resolution of this dataset is currently 0.1° , and the temporal resolution is 3 h. The dataset also provided relative humidity (RH , in percentage) sourced from CMADS V1.1 (the China Meteorological Assimilation Driving Datasets for the SWAT model Version 1.1). This version of the dataset incorporates the STMAS assimilation algorithm, which fuses pre-processed NCEP/GFS background data and automatic station observations using the STMAS algorithm [38]. The spatial resolution of the dataset is 0.25° , and the temporal resolution is daily [39]. Additionally, the data included information on the degree of curing (c , in percentage). The curing values were estimated intuitively as they are not directly measured in the field.

To ensure the accuracy and reliability of the data, real-time meteorological conditions closer to the satellite detection sites and detection times were considered. Fires that were farther away from the site and detection time were excluded from the analysis. After applying the data selection criteria and removing duplicate fires, a total of 29 wildfire observations were included in the dataset for this study. The selected grasslands had a degree of curing (c) greater than 80%. These fires occurred in different seasons and years, with varying environmental factors.

The average wind speed (w) was found to be $17.7 \text{ km} \cdot \text{h}^{-1}$, ranging from 5.7 to $30 \text{ km} \cdot \text{h}^{-1}$. The average air temperature (T) was $9.1 \text{ }^\circ\text{C}$, ranging from -1.1 to $28.9 \text{ }^\circ\text{C}$. The average relative humidity (RH) was 38.1% , ranging from 18.2 to 61.3% . The estimated moisture content (MC) ranged from 10.0 to 16.5% . Table 1 provides basic statistical information for the analyzed dataset.

Table 1. Variable statistics.

Variable	Mean	Range	Unit of Measurement
w	17.7	5.7–30	$\text{km} \cdot \text{h}^{-1}$
T	9.1	1.1–28.9	$^\circ\text{C}$
RH	38.1	18.2–61.3	%
MC	12.9	10.0–16.5	%

3.3. Results

Through model calculations, it was observed that temperature and wind speed exert a positive influence on the extent of fire propagation. Specifically, higher temperatures and increased wind speeds were found to correspond to a larger area of fire spread. Conversely, relative humidity exhibited an inverse relationship, with higher moisture content leading to a deceleration in the rate of fire spread. The outcomes derived from this model will be juxtaposed with the field-measured data in the Hulunbuir Grassland. Furthermore, this study includes a comparison with Li's [28] and Zhou's [25] models for comprehensive analysis. The Pearson correlation coefficient (R) was selected as the method for comparing the accuracy of several models. Table 2 and Figure 8 present the corresponding results obtained using our model, which demonstrate a higher level of consistency with the observed fire spread speed in the Hulunbuir Grassland. In contrast, Li's model and Zhou's model, which also incorporate fire speed measurements to estimate fire area, were selected and evaluated using the same fire data (Figure 9).

Table 2. The fire spread speed.

Speed	Mean	Range	Unit of Measurement
u_p	1.99	1.11–3.03	$\text{km} \cdot \text{h}^{-1}$
u_b	1.55	0.35–2.33	$\text{km} \cdot \text{h}^{-1}$
v	0.43	0.26–0.57	$\text{km} \cdot \text{h}^{-1}$

To verify the effectiveness of the model, five fires of varying intensities that occurred in different locations within the Inner Mongolia Autonomous Region between 2015 and 2023 were selected for analysis. The predicted fire spread areas generated by three distinct models, including the model proposed in this paper, were compared with the actual fire spread areas (see Table 3 and Figure 10). The results demonstrate that our model closely aligns with the actual fire outcomes. In contrast, the values projected by Li's and Zhou's models tend to underestimate the actual fire outcomes.

Table 3. Comparison of actual fire spread area and model-predicted fire spread area.

Location	Time	Actual Area	New Model	Li's	Zhou's
Manzhouli City	16 April 2015	59.99	60.29	4.44	0.77
Old Barag Banner	17 May 2017	33.56	30.35	0.20	0.61
New Barag Left Banner	11 September 2022	71.62	73.94	0.48	1.57
East Ujimqin Banner	8 April 2023	601.69	606.44	12.28	19.64
Old Barag Banner	1 May 2023	100.32	106.37	1.61	1.57

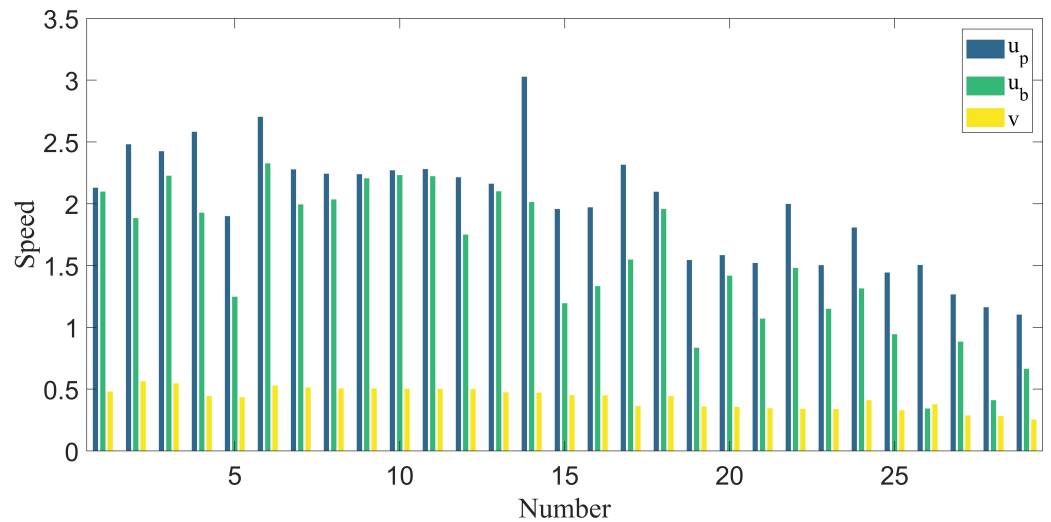


Figure 8. The computed fire spread speed.

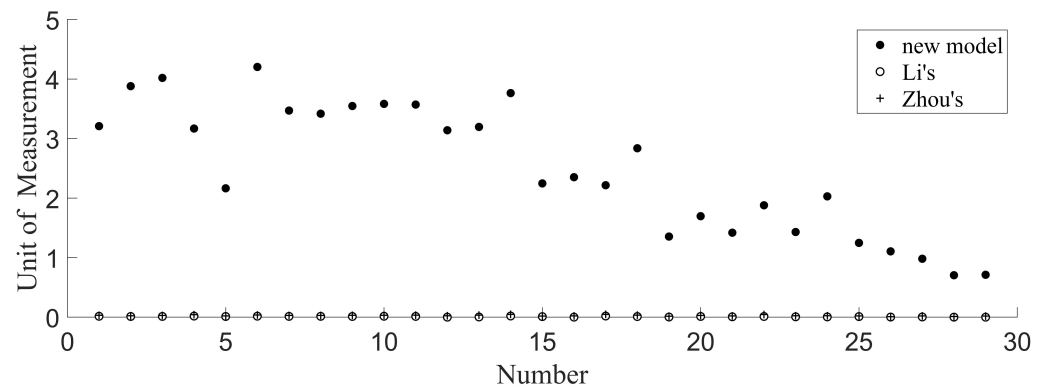


Figure 9. The comparison of the calculations per unit fire spread area among three models.

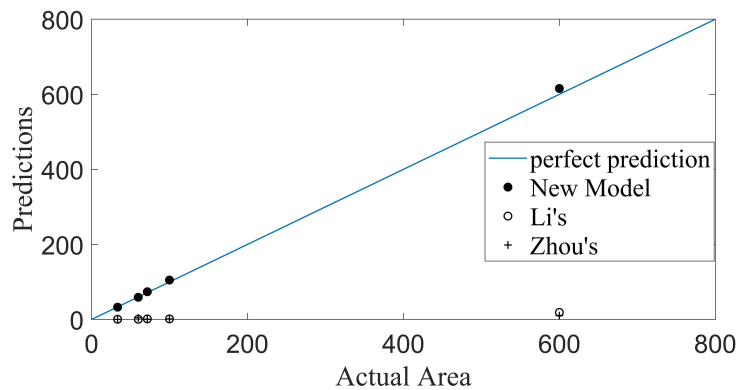


Figure 10. Comparison of observed fire spread area and model-predicted fire spread area.

3.4. Comparison of Models

Li's model represents a class of moderately complex models. It is rooted in the fire occurrence process, incorporating constraints such as fuel moisture and wind speed. This model is integrated within the Dynamic Global Vegetation Model IAP-DGVM. It has demonstrated strong performance in simulating global carbon fluxes. Zhou's study in the Hulunbuir Grassland shares the same experimental area as the present article. Zhou's study resulted in the development of a model for quantifying fire area. By comparing with theirs, the results indicate the superiority of our model. The correlation coefficients between the fire radiative power and the fire spread area per unit of time, as simulated by Zhou's and Li's models, are 0.3498 and 0.3817, respectively. The correlation coefficient between the fire spread area per unit of time and the fire radiative power, as simulated by the coupled model, is 0.6016.

We evaluated the performance of the new fire parameterization scheme by comparing its simulation results with those of the fire parameterization models developed by Li and Zhou. The results demonstrate that the correlation between the simulated average burning area per unit of time (new model: $Cor = 0.6016$) and fire radiative power is higher than the correlation between Li's and Zhou's fire models (old models: $Cor = 0.3817$, $Cor = 0.3498$) and fire radiative power. Compared to Li's and Zhou's fire parameterization models, the new fire parameterization not only provides more accurate simulations of fire spread rate and area but also exhibits a higher correlation with fire radiative power in terms of fire spread area per unit of time. These findings indicate that the new fire parameterization scheme can improve fire simulation accuracy.

A prominent characteristic of this model is its suitability for simulating and predicting fire occurrences on a small scale at specific locations, as the data utilized is specific to those individual points, rendering it a point-to-point model. The development of this fire model in our study offers a method for quickly assessing and predicting fire spread speed and area. This model enables the establishment of a rapid relationship between real-time conditions and fire behavior. The inclusion of a small number of parameters in the model assists firefighters in better calculating and predicting fire spread. The model is applicable throughout the day and can predict fires in different months. Furthermore, the results of our study have broader implications beyond operational fire spread prediction. The validation of the fire model using fire radiative power in the Hulunbuir Grassland demonstrates its suitability for analyzing fire occurrence in this region (Pearson correlation coefficient: 0.6016).

3.5. Evaluation

Our model employs an innovative approach by integrating Li's and Miguel's models to address the challenge of fire measurement on smaller scales. The proposed model demonstrates improved accuracy in estimating fire spread, computational efficiency, and enhanced interpretability. These advancements contribute to a better understanding of fire behavior and enable more effective fire control measures, particularly in the context of the Hulunbuir Grassland fire. Additionally, the new fire parameterization model in this study provides specific and feasible function formulas for calculating the fire spread rate in all directions, including the downwind direction, upwind direction, and perpendicular to the wind direction. Li's and Zhou's models provide detailed descriptions of the two fire parameterization scenarios, respectively. Compared to the coupled model in this paper, both Li's and Zhou's tend to underestimate the fire spread rate and fire spread area per unit of time. This can be seen in Figure 9. The robust generalization capability of the current model is evidenced through simulations conducted in various regions of Inner Mongolia, excluding Hulunbuir.

In the contemporary context, human management of fire is on the rise, owing to advancements in fire detection and suppression technologies. Fire, as a natural force, presents a dual nature: while it can have detrimental effects on the environment and resources, controlled fires can expedite the regeneration of grassland ecosystems and

stimulate vegetation growth. Accurate quantification of fire dynamics holds the potential to enhance fire management strategies, effectively curbing fire spread while simultaneously addressing human requirements. The application of this model to analyze small-scale grassland fires holds promise for facilitating the prediction and management of such fires, thereby contributing to a deeper comprehension of the carbon cycle within grassland ecosystems and terrestrial ecosystems at large.

The error level ascertained from this model demonstrates a lower magnitude in comparison to assessments made by alternative models. Our chosen Hulunbuir Grasslands exhibit a predominantly flat terrain, distinguishing them from areas characterized by forests, bushes, or other topographies. Consequently, topographic influences are relatively minimal in this region. In such flat landscapes, the velocity of wind holds significant sway over the propagation of fires, a factor that our model delves into comprehensively. It is important to note that our current analysis is focused solely on the Hulunbuir region. Nevertheless, the diversity in grass fuel composition across semi-arid, grassland, and temperate regions globally, where grass fires are prevalent, mirrors the spectrum of conditions found in Hulunbuir [40,41]. Hence, based on the similarity in fuel structure, no apparent constraints limit the application of our model solely to the Hulunbuir Grasslands [42–45].

Similar grasslands thriving in analogous temperate environments with corresponding fuel compositions can be deemed suitable for the utilization of our model. The model necessitates only four key input variables: temperature, precipitation, wind speed, and curing degree. Once the current time's data (or daily average) is accessible, the model can effectively estimate the rate of fire spread. In this light, the model can be integrated into a broader system seamlessly, provided the necessary input variables are at hand. However, it is essential to acknowledge that the model's efficacy lies in assessing fires that have transpired or are ongoing; it cannot effectively predict situations where fires do not occur.

4. Conclusions

In this paper, we have developed a process-based medium-complexity fire parameterization scheme. It is suitable for small-scale fine-scale change studies. We identified wind speed as a crucial factor influencing fire spread rate. By considering the relationship between the spreading direction and wind direction, we decomposed the fire spread rate into three categories: downwind spreading rate, upwind spreading rate, and rate perpendicular to the wind direction. Furthermore, we incorporated the influence of environmental factors, such as temperature and relative humidity, into the calculation model for fire downwind spread rate. Assuming the post-fire area to be elliptical, we determined the relationship between fire spread rates using mathematical properties of ellipses and derived parametric equations for the three types of fire spread rates. The burning area of a fire is determined by the average fire spread rate and fire duration, and the burning area per unit of time is estimated from the fire spread velocity. Environmental factors, such as wind speed, are incorporated into the calculation of fire spread speed, enhancing the mathematical approaches for the quantitative investigation of grassland fires and expanding the possibilities for studying such fires.

The time unit utilized in this model for predicting fire area is the hour. Consequently, more accurate predictions are achievable when the forecast duration exceeds half an hour or more. For fires of shorter duration, particularly those characterized by minor area fluctuations due to varying wind speeds, the model's ability to capture these nuances is limited. This model primarily focuses on the impact of wind speed on the spread of fires. It is imperative to ensure the consistency of wind direction when analyzing real-world scenarios and utilizing this model. The applicability of this model is hindered in cases where wind direction fluctuates during the progression of a fire. This model demonstrates superior capabilities in enhancing the precision of fire spread area estimation. By refining the accuracy of fire spread area determination, the spatial scope of model calculations can be effectively constrained. In the context of air quality (AQ) modeling, the precise delineation of the fire-affected area and the extent of its impact play a pivotal role in shaping

the simulation of fire-related pollutant transport and dispersion within the atmosphere. Enhancing the precision of fire spread area quantification is instrumental in optimizing the efficiency and accuracy of model computations, thereby facilitating more effective atmospheric prediction. The synergistic integration of this model with AQ modeling constitutes a key area of focus for future research endeavors.

In our forthcoming research, it will be imperative to augment the dataset with additional information on grassland wildfires, enabling ongoing evaluation and enhancement of the model using independent data. Furthermore, our focus will encompass the exploration of grassland fire models applicable to a broader spectrum of fire durations. This approach will enable us to forecast and manage a wider array of grassland fires, yielding improved operational outcomes.

Author Contributions: Y.Z.: conceptualization, software, and writing (original draft). H.Y.: methodology and visualization. W.H.: funding acquisition and supervision. T.H.: formal analysis and writing (review and editing). M.F.: resources and data curation. K.W.: conceptualization, formal analysis, and project administration. All authors have read and agreed to the published version of the manuscript.

Funding: This research was funded by the Strategic Priority Research Program of the Chinese Academy of Sciences, Grant No. XDA26010304 and the Project of Northern Agriculture and Livestock Husbandry Technical Innovation Center, Chinese Academy of Agricultural Sciences (BFGJ2022002).

Institutional Review Board Statement: Not applicable.

Informed Consent Statement: Not applicable.

Data Availability Statement: The raw data supporting the conclusions of this article will be made available by the authors on request.

Acknowledgments: The datasets are provided by National Tibetan Plateau/Third Pole Environment Data Center (<http://data.tpdc.ac.cn> (accessed on 27 June 2023)).

Conflicts of Interest: The authors declare no conflicts of interest.

References

1. Bardgett, R.D.; Bullock, J.M.; Lavorel, S.; Manning, P.; Schaffner, U.; Ostle, N.; Shi, H. Combatting global grassland degradation. *Nat. Rev. Earth Environ.* **2021**, *2*, 720–735. [[CrossRef](#)]
2. Feng, Y.; Lu, Q.; Tokola, T.; Liu, H.; Wang, X. Assessment of grassland degradation in Guinan county, Qinghai Province, China, in the past 30 years. *Land Degrad. Dev.* **2009**, *20*, 55–68. [[CrossRef](#)]
3. Liu, H.; Mi, Z.; Lin, L.I.; Wang, Y.; Zhang, Z.; Zhang, F.; He, J.S. Shifting plant species composition in response to climate change stabilizes grassland primary production. *Proc. Natl. Acad. Sci. USA* **2018**, *115*, 4051–4056. [[CrossRef](#)] [[PubMed](#)]
4. Smith, M.; Wilkins, K.; Holdrege, M.; Wilfahrt, P.; Collins, S.; Knapp, A.; Sala, O.; Dukes, J.; Phillips, R.; Yahdjian, L.; et al. Extreme drought impacts have been underestimated in grasslands and shrublands globally. *Proc. Natl. Acad. Sci. USA* **2024**, *121*, e2309881120. [[CrossRef](#)] [[PubMed](#)]
5. Cochrane, M. Fire Science for Rainforests. *Nature* **2003**, *421*, 913–919. [[CrossRef](#)]
6. East, A.; AghaKouchak, A.; Caprarelli, G.; Filippelli, G.; Fabio, F.; Luce, C.; Rajaram, H.; Russell, L.; Santin, C.; Santos, I. Fire in the Earth System: Introduction to the Special Collection. *J. Geophys. Res. Earth Surf.* **2023**, *128*. [[CrossRef](#)]
7. Che, M.; Chen, B.; Wang, Y.; Guo, X. Review of dynamic global vegetation models (DGVMs). *Chin. J. Appl. Ecol.* **2014**, *25*, 263–271.
8. Huang, X.; Li, H.; Li, X.; Zhang, L. Fire numerical simulation analysis for large-scale public building in 3D GIS. In Proceedings of the IGARSS 2019—2019 IEEE International Geoscience and Remote Sensing Symposium, Yokohama, Japan, 28 July–2 August 2019; pp. 7522–7525.
9. Kelly, R.; Chipman, M.; Higuera, P.; Stefanova, V.; Brubaker, L.; Hu, F. Recent burning of boreal forests exceeds fire regime limits of the past 10,000 years. *Proc. Natl. Acad. Sci. USA* **2013**, *110*, 13055–13060. [[CrossRef](#)] [[PubMed](#)]
10. Xu, D.; Chen, B.; Shen, B.; Wang, X.; Yan, Y.; Xu, L.; Xin, X. The classification of grassland types based on object-based image analysis with multisource data. *Rangel. Ecol. Manag.* **2019**, *72*, 318–326. [[CrossRef](#)]
11. Moritz, M.; Batllori, E.; Bradstock, R.; Gill, M.; Handmer, J.; Hessburg, P.; Leonard, J.; Mccaffrey, S.; Odion, D.; Schoennagel, T.; et al. Learning to coexist with wildfire. *Nature* **2014**, *515*, 58–66. [[CrossRef](#)] [[PubMed](#)]
12. McWethy, D.B.; Schoennagel, T.; Higuera, P.E.; Krawchuk, M.A.; Harvey, B.J.; Metcalf, E.C.; Schultz, C.A.; Miller, C.; Metcalf, A.L.; Buma, B.J.; et al. Rethinking resilience to wildfire. *Nat. Sustain.* **2019**, *2*, 797–804. [[CrossRef](#)]
13. Lu, C.; Sun, Y.; Wan, H.; Zhang, X.; Yin, H. Anthropogenic influence on the frequency of extreme temperatures in China: Anthropogenic influence on extremes. *Geophys. Res. Lett.* **2016**, *43*, 6511–6518. [[CrossRef](#)]

14. Davis, K.; Dobrowski, S.; Higuera, P.; Holden, Z.; Veblen, T.; Rother, M.; Parks, S.; Sala, A.; Maneta, M. Wildfires and climate change push low-elevation forests across a critical climate threshold for tree regeneration. *Proc. Natl. Acad. Sci. USA* **2019**, *116*, 6193–6198. [[CrossRef](#)]
15. Walker, X.; Baltzer, J.; Cumming, S.; Day, N.; Ebert, C.; Goetz, S.; Johnstone, J.; Potter, S.; Rogers, B.; Schuur, E.; et al. Increasing wildfires threaten historic carbon sink of boreal forest soils. *Nature* **2019**, *572*, 520–523. [[CrossRef](#)] [[PubMed](#)]
16. Marlon, J.; Bartlein, P.; Carcaillet, C.; Gavin, D.; Harrison, S.; Higuera, P.; Joos, F.; Power, M.; Prentice, I. Erratum: Climate and human influences on global biomass burning over the past two millennia. *Nat. Geosci.* **2008**, *1*, 697–702. [[CrossRef](#)]
17. Trouet, V.; Taylor, A.; Wahl, E.; Skinner, C.; Stephens, S. Fire-Climate Interactions in the American West Since 1400 CE. *Geophys. Res. Lett.* **2010**, *37*. [[CrossRef](#)]
18. Flannigan, M.; Krawchuk, M.; Wotton, M.; Johnston, L. Implications of changing climate for global Wildland fire. *Int. J. Wildland Fire* **2009**, *18*, 483–507. [[CrossRef](#)]
19. Ganteaume, A.; Camia, A.; Jappiot, M.; San-Miguel-Ayanz, J.; Long-Fournel, M.; Lampin, C. A Review of the Main Driving Factors of Forest Fire Ignition Over Europe. *Environ. Manag.* **2012**, *51*, 651–662. [[CrossRef](#)] [[PubMed](#)]
20. Doerr, S.; Santin, C. Global trends in wildfire and its impacts: Perceptions versus realities in a changing world. *Philos. Trans. R. Soc. B Biol. Sci.* **2016**, *371*, 20150345. [[CrossRef](#)] [[PubMed](#)]
21. Prichard, S.; Stevens-Rumann, C.; Hessburg, P. Tamm Review: Shifting global fire regimes: Lessons from reburns and research needs. *For. Ecol. Manag.* **2017**, *396*, 217–233. [[CrossRef](#)]
22. Luke, R.H.; McArthur, A.G. *Bushfires in Australia*; Australian Government Publishing Service for CSIRO: Canberra, Australia, 1978.
23. Burrows, N. Introduction to McArthur and Cheney's Article. *Fire Ecol.* **2015**, *11*, 1–2. [[CrossRef](#)]
24. Cheney, N.P.; Gould, J.S.; Catchpole, W.R. Prediction of fire spread in grasslands. *Int. J. Wildland Fire* **1998**, *8*, 1–13. [[CrossRef](#)]
25. Zhou, D.W.; Zhang, Z.S. Grass fire burning, fire behavior, and fire climate. *Chin. J. Grassl.* **1996**, *3*, 74–77.
26. Cruz, M.G.; Alexander, M.E.; Kilinc, M. Wildfire rates of spread in grasslands under critical burning conditions. *Fire* **2022**, *5*, 55. [[CrossRef](#)]
27. Arora, V.K.; Boer, G.J. Fire as an interactive component of dynamic vegetation models. *J. Geophys. Res. Biogeosci.* **2005**, *110*. [[CrossRef](#)]
28. Li, F.; Zeng, X.D.; Levis, S. A process-based fire parameterization of intermediate complexity in a Dynamic Global Vegetation Model. *Biogeosciences* **2012**, *9*, 2761–2780. [[CrossRef](#)]
29. Bao, G.; Liu, Y.; Linderholm, H.W. April–September mean maximum temperature inferred from Hailar pine (*Pinus sylvestris* var. *mongolica*) tree rings in the Hulunbuir region, Inner Mongolia, back to 1868 AD. *Palaeogeogr. Palaeoclimatol. Palaeoecol.* **2012**, *313*, 162–172. [[CrossRef](#)]
30. Zhang, Q.; Tang, H.; Cui, F.; Dai, L. SPEI-based analysis of drought characteristics and trends in Hulun Buir grassland. *Acta Ecol. Sin.* **2019**, *39*, 7110–7123.
31. Zhang, G.; Xu, X.; Zhou, C.; Zhang, H.; Ouyang, H. Responses of grassland vegetation to climatic variations on different temporal scales in Hulun Buir Grassland in the past 30 years. *J. Geogr. Sci.* **2011**, *21*, 634–650. [[CrossRef](#)]
32. Fang, K.; Yao, Q.; Guo, Z.; Zheng, B.; Du, J.; Qi, F.; Yan, P.; Li, J.; Ou, T.; Liu, J.; et al. ENSO modulates wildfire activity in China. *Nat. Commun.* **2021**, *12*, 1764. [[CrossRef](#)] [[PubMed](#)]
33. Xing, H.; Fang, K.; Yao, Q.; Zhou, F.; Ou, T.; Liu, J.; Zhou, S.; Jiang, S.; Chen, Y.; Bai, M.; et al. Impacts of changes in climate extremes on wildfire occurrences in China. *Ecol. Indic.* **2023**, *157*, 111288. [[CrossRef](#)]
34. Roy, D.P.; Kumar, S.S. Multi-year MODIS active fire type classification over the Brazilian Tropical Moist Forest Biome. *Int. J. Digit. Earth* **2017**, *10*, 54–84. [[CrossRef](#)]
35. Li, F.; Zhang, X.; Kondragunta, S.; Csiszar, I. Comparison of Fire Radiative Power Estimates From VIIRS and MODIS Observations. *J. Geophys. Res. Atmos.* **2018**, *123*, 4545–4563. [[CrossRef](#)]
36. He, J.; Yang, K.; Tang, W.; Lu, H.; Qin, J.; Chen, Y.; Li, X. The first high-resolution meteorological forcing dataset for land process studies over China. *Sci. Data* **2020**, *7*, 25. [[CrossRef](#)] [[PubMed](#)]
37. Yang, K.; He, J.; Tang, W.; Qin, J.; Cheng, C. On downward shortwave and longwave radiations over high altitude regions: Observation and modeling in the Tibetan Plateau. *Agric. Forest. Meteorol.* **2010**, *150*, 38–46. [[CrossRef](#)]
38. Meng, X.Y.; Wang, H.; Wu, Y.P.; Long, A.H.; Wang, J.H.; Shi, C.X.; Ji, X.N. Investigating spatiotemporal changes of the land surface processes in Xinjiang using high-resolution CLM3.5 and CLDAS: Soil temperature. *Sci. Rep.* **2017**, *7*, 13286. [[CrossRef](#)] [[PubMed](#)]
39. Meng, X.; Ji, X.; Liu, Z. Energy Balance-Based SWAT Model to Simulate the Mountain Snowmelt and Runoff—Taking the Application in Juntanghu Watershed (China) as an Example. *J. Mt. Sci.* **2015**, *12*, 368–381. [[CrossRef](#)]
40. Smit, I.P.; Archibald, S. Herbivore culling influences spatio-temporal patterns of fire in a semiarid savanna. *J. Appl. Ecol.* **2019**, *56*, 711–721. [[CrossRef](#)]
41. Trollope, W.; Potgieter, A. Estimating grass fuel loads with a disc pasture meter in the Kruger National Park. *J. Grassl. Soc. South. Afr.* **1986**, *3*, 148–152. [[CrossRef](#)]
42. Van Wilgen, B.W.; Wills, A. Fire behaviour prediction in savanna vegetation. *S. Afr. J. Wildl. Res.* **1988**, *18*, 41–46.
43. Scott, J.H. *Standard fire Behavior Fuel Models: A Comprehensive Set for Use with Rothermel's Surface Fire Spread Model*; U.S. Department of Agriculture, Forest Service, Rocky Mountain Research Station: Fort Collins, CO, USA, 2005.

44. McGranahan, D.A.; Engle, D.M.; Miller, J.R.; Debinski, D.M. An invasive grass increases live fuel proportion and reduces fire spread in a simulated grassland. *Ecosystems* **2013**, *16*, 158–169. [[CrossRef](#)]
45. Miller, C.; Plucinski, M.; Sullivan, A.; Stephenson, A.; Huston, C.; Charman, K.; Prakash, M.; Dunstall, S. Electrically caused wildfires in Victoria, Australia are over-represented when fire danger is elevated. *Landsc. Urban Plan.* **2017**, *167*, 267–274. [[CrossRef](#)]

Disclaimer/Publisher’s Note: The statements, opinions and data contained in all publications are solely those of the individual author(s) and contributor(s) and not of MDPI and/or the editor(s). MDPI and/or the editor(s) disclaim responsibility for any injury to people or property resulting from any ideas, methods, instructions or products referred to in the content.